

ACCEPTED MANUSCRIPT

Epitaxial growth of quasi-one-dimensional TaNi₂Se₂ monolayer with anisotropic electronic and mechanical properties

To cite this article before publication: Jiayi Wang *et al* 2026 *Chinese Phys. B* in press <https://doi.org/10.1088/1674-1056/ae5a15>

Manuscript version: Accepted Manuscript

Accepted Manuscript is “the version of the article accepted for publication including all changes made as a result of the peer review process, and which may also include the addition to the article by IOP Publishing of a header, an article ID, a cover sheet and/or an ‘Accepted Manuscript’ watermark, but excluding any other editing, typesetting or other changes made by IOP Publishing and/or its licensors”

This Accepted Manuscript is © 2026 Chinese Physical Society and IOP Publishing Ltd.



During the embargo period (the 12 month period from the publication of the Version of Record of this article), the Accepted Manuscript is fully protected by copyright and cannot be reused or reposted elsewhere.

As the Version of Record of this article is going to be / has been published on a subscription basis, this Accepted Manuscript will be available for reuse under a CC BY-NC-ND 4.0 licence after the 12 month embargo period.

After the embargo period, everyone is permitted to use copy and redistribute this article for non-commercial purposes only, provided that they adhere to all the terms of the licence <https://creativecommons.org/licenses/by-nc-nd/4.0>

Although reasonable endeavours have been taken to obtain all necessary permissions from third parties to include their copyrighted content within this article, their full citation and copyright line may not be present in this Accepted Manuscript version. Before using any content from this article, please refer to the Version of Record on IOPscience once published for full citation and copyright details, as permissions may be required. All third party content is fully copyright protected, unless specifically stated otherwise in the figure caption in the Version of Record.

View the [article online](#) for updates and enhancements.

1 Epitaxial growth of quasi-one-dimensional TaNi₂Se₂ monolayer with
2 anisotropic electronic and mechanical properties
3

4 Jiayi Wang (王嘉翌)^{1,2#}, Qiuchen Yu (余秋辰)^{1,2#}, Hui Guo (郭辉)^{1,2#*}, Peng Fan (范朋)^{1,2}, Siyu Xu (徐
5 思宇)², Yixuan Gao (高艺璇)^{3*}, Hui Chen (陈辉)^{1,2*}, and Hong-Jun Gao (高鸿钧)^{1,2}
6

7 ¹ *Beijing National Center for Condensed Matter Physics and Institute of Physics, Chinese Academy of
8 Sciences, Beijing 100190, China*

9 ² *School of Physical Sciences, University of Chinese Academy of Sciences, Beijing 100190, China*

10 ³ *State Key Laboratory for Advanced Metals and Materials, University of Science and Technology
11 Beijing, Beijing 100083, China*

12
13
14
15
16 #These authors contributed equally to this work

17 *Correspondence to: hchenn04@iphy.ac.cn, guohui@iphy.ac.cn, gaoyixuan@ustb.edu.cn
18
19
20
21
22

1 **Abstract**

2 Quasi-one-dimensional (quasi-1D) van-der-Waals layered materials have garnered significant interest
3 for their intrinsic in-plane anisotropy and potential applications in low-dimensional quantum devices.
4 Here, we report the realization of a quasi-1D TaNi₂Se₂ monolayer with pronounced anisotropic electronic
5 and mechanical properties. The monolayer TaNi₂Se₂ is synthesized on a graphite substrate via van-der-
6 Waals epitaxy. Using low-temperature scanning tunneling microscopy/spectroscopy, we reveal the
7 characteristic quasi-1D chain-like lattice structure and confirm the intrinsic metallic nature of the
8 monolayer TaNi₂Se₂. Notably, the electronic states exhibit a pronounced quasi-1D modulation that
9 follows the chain structure, indicating strong electronic anisotropy. First-principles calculations further
10 confirm the structural stability and provide signatures of anisotropic in-plane mechanical properties, as
11 well as possible topological edge states arising from spin-orbit coupling. Our findings establish
12 monolayer TaNi₂Se₂ as a novel quasi-1D van-der-Waals material and provide a promising platform for
13 exploring anisotropy-driven quantum phenomena and device applications.

14
15
16 **Keywords**

17 Quasi-1D, TaNi₂Se₂ monolayer; Anisotropy; Epitaxial growth; Scanning tunneling microscopy

18
19 **PACS**

20 73.22.-f; 68.37.Ef; 81.15.Hi; 62.20.de

1 Introduction

2 The exploration of two-dimensional (2D) materials has evolved from high-symmetry systems, such as
3 graphene^[1-4] and hexagonal transition metal dichalcogenides (TMDs),^[5-8] to those exhibiting lower in-
4 plane symmetry, such as black phosphorus,^[9,10] ReS₂,^[11,12] and WTe₂.^[13,14] Lowering crystal symmetry
5 can introduce new physical degrees of freedom, enabling phenomena such as in-plane anisotropic
6 transport,^[15,16] linear dichroism,^[17,18] and piezoelectricity.^[19,20] Among these low-symmetry materials, a
7 particularly intriguing subclass consists of compounds composed of atomic chains weakly coupled by
8 inter-chain interactions, representing the extreme limit of in-plane anisotropy. These quasi-one-
9 dimensional (quasi-1D) systems bridge the physics of 2D and 1D materials, offering a fertile platform
10 for exploring phenomena associated with reduced dimensionality, including Peierls instability,^[21,22]
11 sliding charge density waves (CDWs) in NbSe₃,^[23,24] CDW-tuned vortex bound states in 1T'-NbTe₂,^[25]
12 and possible topological superconductivity in TaSe₃.^[26] Consequently, discovering new quasi-1D van-
13 der-Waals (vdW) materials has become an important frontier for exploring exotic quantum phases.

14
15 Within the family of quasi-1D vdW systems, the ternary chalcogenide family TaM₂X₂ (X = Te, Se; M =
16 Ni, Co) is distinguished by its rich phase diagram hosting diverse electronic and magnetic states.^[27-32]
17 For instance, TaNi₂Te₂ has been identified to exhibit canted antiferromagnetism,^[27] while TaCo₂Te₂
18 displays air-stable metallic ferromagnetism with high carrier mobility,^[30] as well as large
19 magnetoresistance and quantum oscillations.^[29] However, the current studies have predominantly
20 focused on telluride compounds, leaving the selenium-based analogue largely unexplored. Investigating
21 the Te-to-Se substitution is particularly intriguing because the smaller atomic radius of Se effectively
22 introduces a chemical pressure effect.^[33] This structural contraction is expected to modify inter-chain
23 hopping and electron correlations, characterized by the ratio between Coulomb interaction and
24 bandwidth (U/W), potentially driving the system toward a quantum ground state distinct from the
25 telluride counterparts.^[34,35]

26
27 In this work, we report the realization of a quasi-1D TaNi₂Se₂ monolayer grown on highly oriented
28 pyrolytic graphite (HOPG) using molecular beam epitaxy (MBE). Low-temperature scanning tunneling
29 microscopy and spectroscopy (STM/STS) measurements reveal the formation of a well-ordered chain-
30 like lattice structure and confirm the intrinsic metallic nature of the monolayer. Remarkably, the

1 electronic states exhibit pronounced quasi-1D modulation following the atomic chains, directly
2 demonstrating strong electronic anisotropy. Combined with first-principles calculations, we further
3 confirm the structural stability of the monolayer and predict anisotropic in-plane mechanical responses,
4 together with possible topological edge states induced by spin-orbit coupling. Our results establish
5 monolayer TaNi₂Se₂ as a new member of quasi-1D vdW materials and provide a promising platform for
6 investigating anisotropy-driven quantum phenomena.

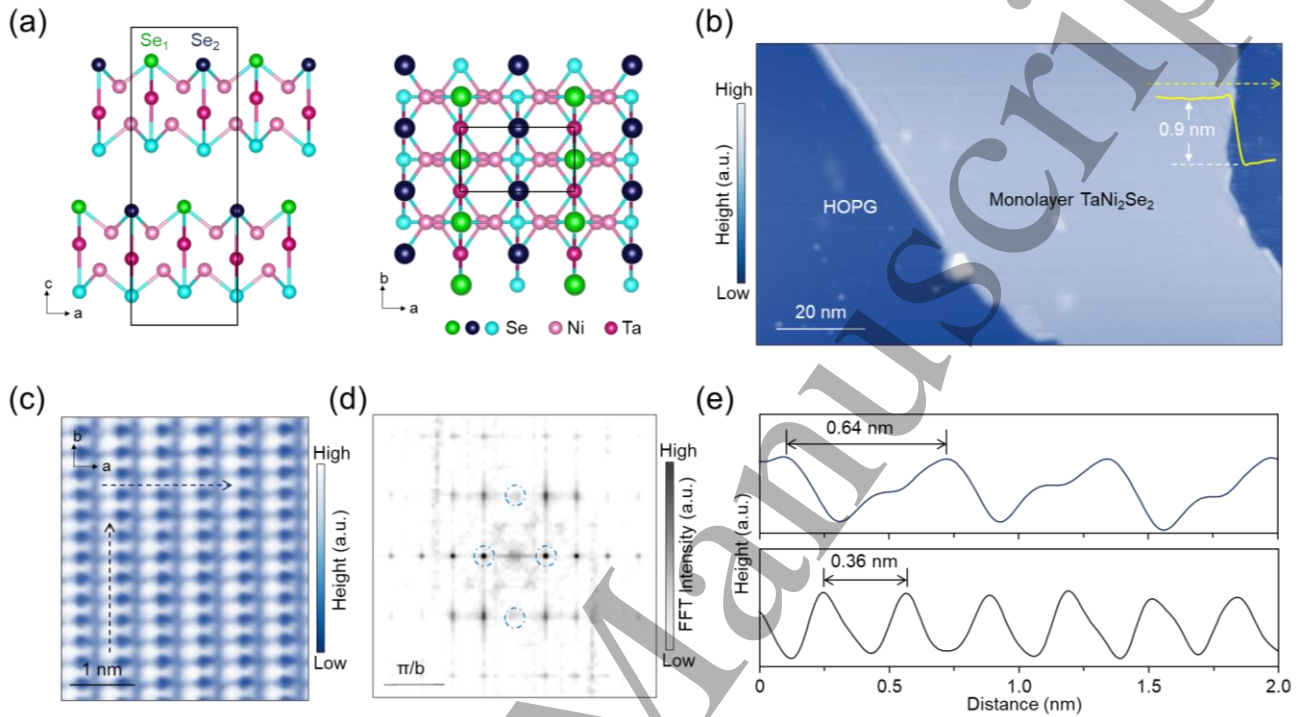
8 **Results and discussion**

9 Figure 1(a) illustrates the crystal structure of the TaNi₂Se₂, which crystalizes in an orthorhombic lattice
10 belonging to the space group *Pnma* (No. 62). As shown in the side view model, the TaNi₂Se₂ features a
11 sandwich-like structure where a metallic Ta-Ni sub-layer is sandwiched between two selenium atomic
12 sheets. A distinctive structural motif of this phase is the presence of quasi-1D Ta-Ni chains running along
13 the crystallographic *b*-axis. Within these chains, the Ta atoms are coordinated in a distorted monocapped
14 pentagonal prismatic geometry formed by Se atoms,^[36] giving rise to a corrugated surface profile.
15 Consequently, the topmost Se atoms occupy two crystallographically inequivalent sites along the *a*-axis.

16
17 The monolayer TaNi₂Se₂ is grown on HOPG substrate via vdW epitaxy, a widely used approach for
18 synthesizing 2D layered materials on inert substrates,^[37] where the weak interfacial interaction does not
19 require lattice matching while still enabling preferred in-plane orientations.^[38-40] In addition, as an inert
20 vdW substrate with minimal coupling, HOPG largely preserves the intrinsic structural and electronic
21 properties of monolayer TaNi₂Se₂. Figure 1(b) presents a typical large-scale STM topographic image of
22 the as-grown monolayer TaNi₂Se₂. The apparent step height is approximately 0.9 nm, indicating the
23 monolayer thickness. The atomically-resolved STM image shown in Fig. 1(c) reveals a surface
24 morphology dominated by parallel atomic chains. The observed atomic arrangement is consistent with
25 the structural model presented in Fig. 1(a) and resembles the lattice features previously reported in STM
26 studies of TaNi₂Te₂ and TaCo₂Te₂.^[28] To quantitatively determine the lattice periodicity, we performed a
27 Fast Fourier Transform (FFT) analysis on the atomic-resolution image. The resulting FFT pattern (Fig.
28 1(d)) exhibits sharp Bragg spots arranged in a rectangular symmetry (marked by blue circles),
29 corroborating the high crystallinity and the orthorhombic symmetry of the TaNi₂Se₂. Lattice constants
30 extracted from the line profiles along the principal axes (Fig. 1(e)) yield *a*~0.64 nm and *b*~0.36 nm, in

1 good agreement with the optimized lattice parameters obtained from our density functional theory (DFT)
 2 calculations, which give $a=0.65$ nm and $b=0.35$ nm for the freestanding monolayer TaNi_2Se_2 .

3



4

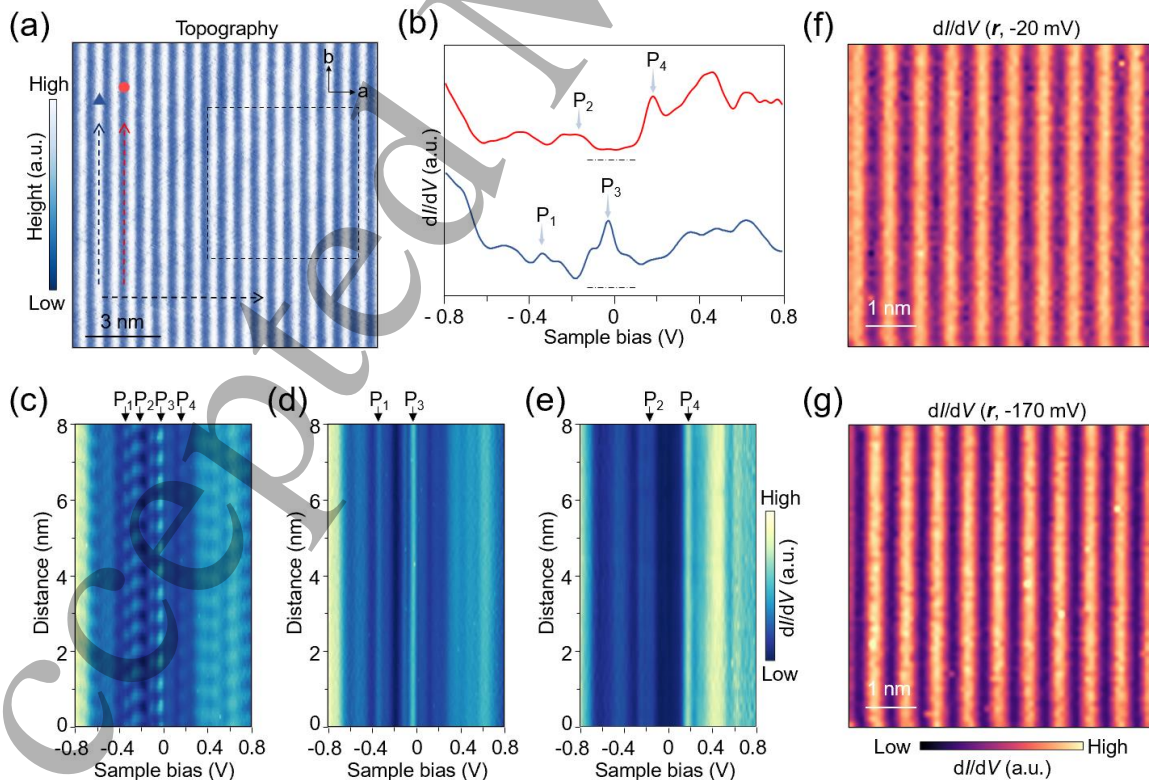
5

6 **Fig. 1.** Structural characterizations of monolayer TaNi_2Se_2 on HOPG substrate. (a) Side and top views of the crystal
 7 structure of TaNi_2Se_2 , showing a vdW layered structure composed of quasi-1D atomic chains. The topmost Se atoms
 8 colored in orange and blue distinguish the two crystallographic inequivalent sites. (b) Large-scale STM topographic
 9 image of a monolayer TaNi_2Se_2 film ($V_s = 2$ V, $I_t = 100$ pA). The inset displays the height profile measured along the
 10 yellow dashed line, showing a step height of approximately 0.9 nm. (c) Atomically-resolved STM image ($V_s = 5$ mV, I_t
 11 $= 3$ nA), revealing the quasi-1D lattice structure. (d) The FFT pattern of (c), where the blue circles mark the Bragg
 12 diffraction spots arranged in a rectangular symmetry. (e) Height profiles extracted along the white (perpendicular to
 13 chains, a -axis) and black (parallel to chains, b -axis) dashed arrows in (c), yielding lattice constants of $a \sim 0.64$ nm
 14 $b \sim 0.36$ nm, respectively.

15

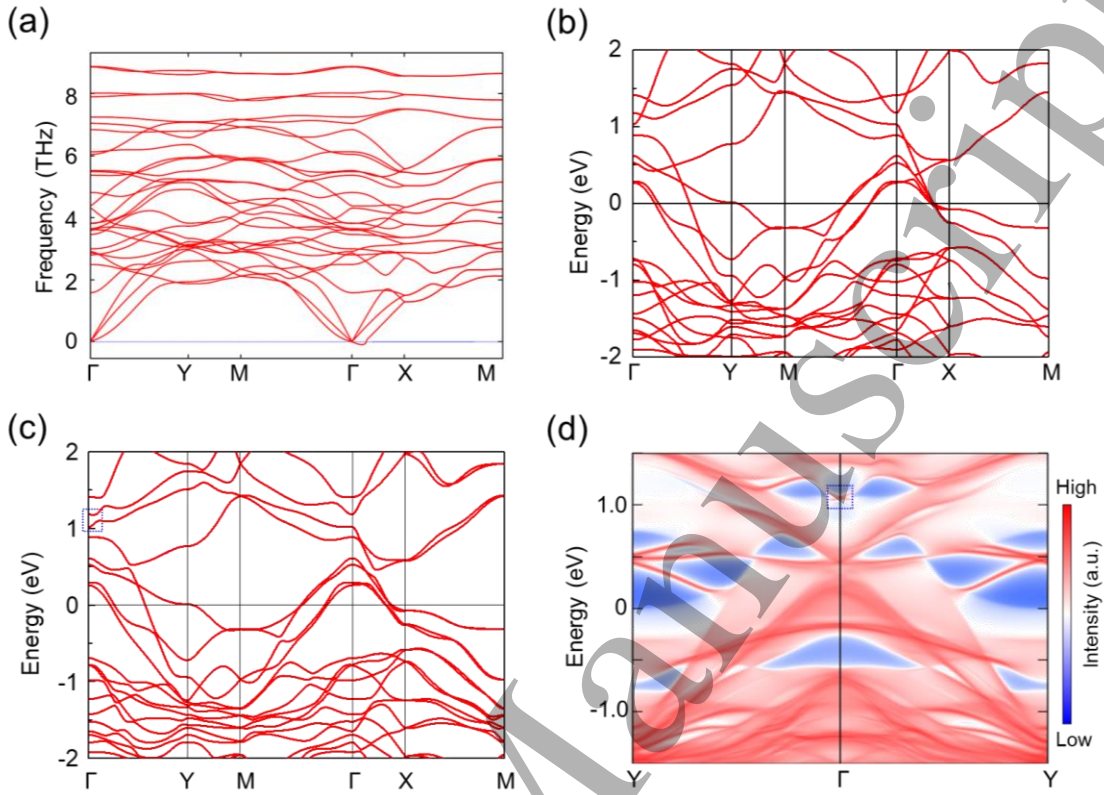
16 We next investigate the electronic properties of the as-grown monolayer TaNi_2Se_2 . Figure 2(a) presents
 17 a typical STM topographic image, where the characteristic chain-like stripes along the b -axis are clearly
 18 resolved. The dI/dV spectra acquired on two distinct stripes, i.e., the bright and dark stripes, both exhibit
 19 finite density of states at the Fermi level, providing direct experimental evidence of metallic nature of

1 the monolayer TaNi_2Se_2 (Fig. 2(b)). Notably, the relative intensities of the four prominent peaks near the
 2 Fermi level, labeled P_1 - P_4 , vary significantly between the two distinct stripes. Specifically, the electronic
 3 states near P_1 and P_3 are strongly enhanced on the bright stripe but suppressed on the dark stripe, whereas
 4 those near P_2 and P_4 display the opposite behavior, indicating pronounced spatial modulation of the local
 5 electronic states within the unit cell. To visualize the spatial distribution of these electronic states, a dI/dV
 6 linecut taken across the stripes exhibits clear periodic modulations within the unit cell (Fig. 2(c)).
 7 Importantly, the dominant spectral weight alternates between the energies of P_2 and P_3 across the unit
 8 cell, reflecting the distinct orbital contributions from the alternating Ta-Ni chains and the inequivalent
 9 Se environments. In contrast to the linecut across stripes, the dI/dV linecuts taken along both the bright
 10 and dark stripes reveal spectral homogeneity, as shown in Fig. 2(d) and 2(e). This pronounced anisotropy,
 11 strong modulation across the stripe but homogeneity along them, serves as a spectroscopic signature of
 12 the quasi-1D electronic character of the monolayer TaNi_2Se_2 . Furthermore, the dI/dV maps performed at
 13 bias voltages corresponding to peaks P_3 (Fig. 2(f)) and P_2 (Fig. 2(g)) reveal strongly localized stripe-like
 14 electronic features and energy-dependent contrast reversal, further reflecting highly anisotropic
 15 electronic states confined by the quasi-1D structural chains.



1 **Fig. 2.** Anisotropic electronic properties of the monolayer TaNi₂Se₂. (a) STM topography, showing the quasi-1D stripe-
2 like structure characteristics ($V_s = -400$ mV, $I_t = 1.9$ nA). (b) The dI/dV spectra acquired at the bright stripe (blue curve,
3 position marked by blue triangle in (a)) and dark stripe (red curve, position marked by red circle in (a)), showing
4 pronounced difference of the electronic states between the two kinds of stripes. Four characteristic peaks are labeled as
5 P₁-P₄. The zero dI/dV position is indicated by the black dashed lines. (c) The dI/dV linecut taken across the stripes
6 (black dashed arrow in (a)), showing a strong periodic modulation of the electronic states across the bright and dark
7 stripes. (d), (e) The dI/dV linecuts taken along the bright stripe (blue dashed arrow in (a)) and dark stripe (red dashed
8 arrow in (a)), respectively, both showing spatial homogeneity of the electronic states. (f), (g) The dI/dV maps acquired
9 in the region marked by the black square in (a), at energies corresponding to peaks P₃ (f) and P₂ (g), respectively,
10 showing energy-dependent contrast reversal.

11
12 To gain deep insight into the intrinsic properties of monolayer TaNi₂Se₂, we further performed DFT
13 calculations. To evaluate the structural stability of the monolayer, we calculated the phonon dispersion
14 spectrum, as shown in Fig. 3(a). The absence of imaginary frequencies throughout the Brillouin zone
15 confirms the dynamical stability of the monolayer TaNi₂Se₂, consistent with the successful experimental
16 realization of the material. Figure 3(b) presents the calculated electronic band structure of the
17 freestanding monolayer TaNi₂Se₂ without SOC. Multiple bands cross the Fermi level, indicating a
18 metallic ground state, in good agreement with the STS measurements. The metallic behavior mainly
19 arises from the transition metal d -orbitals forming dispersive states near the Fermi level.^[29] Notably, a
20 saddle-point-like band feature appears near the Γ point in the vicinity of the Fermi level, which is
21 expected to induce an enhanced density of states and may contribute to the peak structure (P₃) observed
22 in the STS spectra in Fig. 2(b). When SOC is included, the band structure exhibits noticeable
23 modifications. As shown in Fig. 3(c), SOC lifts the band degeneracy and induces a local energy gap
24 opens at the Γ point approximately 1 eV above the Fermi level (highlighted by the blue dashed box).
25 This gap opening can be attributed to the band anti-crossing effect induced by the strong spin-orbit
26 interaction inherent to the heavy Ta $5d$ orbitals. We further calculate the edge states using a semi-infinite
27 monolayer TaNi₂Se₂. The projected edge band structure (Fig. 3(d)) exhibits emergent edge states that
28 bridges the bulk valence and conduction bands. The appearance of such conducting channels within the
29 SOC gap suggests the existence of topological boundary states. However, the edge-state energy range
30 significantly overlaps with bulk bands rather than residing in a clean global gap, causing the edge
31 contribution to be masked by the bulk density of states and hindering unambiguous experimental
32 identification.



2

3

4 **Fig. 3.** Theoretical calculations of the stability and electronic structure of freestanding monolayer TaNi₂Se₂. (a) Phonon
 5 dispersion spectrum calculated along high-symmetry paths. The absence of imaginary frequencies across the entire
 6 Brillouin zone confirms the dynamic stability of the monolayer TaNi₂Se₂. (b) Electronic band structure calculated
 7 without SOC. The bands crossing the Fermi level E_F indicate a metallic ground state, consistent with the experimental
 8 dI/dV measurements. (c) The calculated band structure with SOC, showing an energy gap opening at the Γ point
 9 approximately 1 eV above the Fermi level (marked by the blue dashed box). (d) Projected edge states using a semi-
 10 infinite TaNi₂Se₂ model, showing emergence of edge states within the SOC-induced gap, bridging the bulk valence and
 11 conduction bands (highlighted by the blue dashed rectangle).

12

13 Finally, we evaluate the mechanical properties of the quasi-1D monolayer TaNi₂Se₂ by calculating its
 14 orientation-dependent elastic constants using DFT. For a 2D orthorhombic system, there are four
 15 independent elastic constants: C_{11} , C_{22} , C_{12} , C_{66} . Our results show that these constants satisfy the Born
 16 criteria, namely $C_{11}C_{22} - C_{12}^2 > 0$ and $C_{11}, C_{22}, C_{66} > 0$, providing further evidence for the
 17 mechanical stability of the TaNi₂Se₂ monolayer, consistent with the phonon dispersion results. Based on
 18 these elastic constants, the orientation-dependent Young's modulus $E(\theta)$, shear modulus $G(\theta)$, and

1 Poisson's ratio $\nu(\theta)$ can be obtained using the following equations:

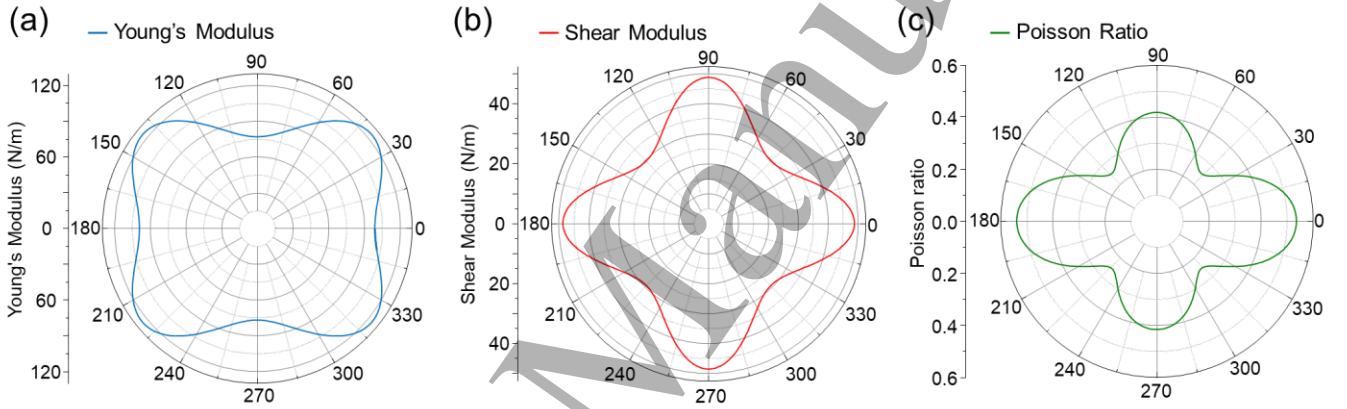
$$E(\theta) = \frac{1}{s_{11}c^4 + (2s_{12} + s_{66})s^2c^2 + s_{22}s^4}$$

$$G(\theta) = \frac{1}{4s_{11}s^2c^2 + 4s_{22}s^2c^2 + 8s_{12}s^2c^2 + s_{66}(s^2 - c^2)^2}$$

$$\nu(\theta) = -\frac{s_{12}(s^4 + c^4) + (s_{11} + s_{22} - s_{66})s^2c^2}{s_{11}c^4 + (2s_{12} + s_{66})s^2c^2 + s_{22}s^4}$$

2 where $c = \cos(\theta)$ and $s = \sin(\theta)$; s_{11} , s_{22} , s_{12} , and s_{66} are the compliance constants derived from the
3 elastic constant matrix.

7



8

9

10 **Fig. 4.** Calculated anisotropic in-plane mechanical properties of monolayer TaNi₂Se₂. (a-c) Polar plots of Young's
11 modulus $E(\theta)$ (a), shear modulus $G(\theta)$ (b), and Poisson's ratio $\nu(\theta)$ (c), showing pronounced mechanical anisotropy of
12 the TaNi₂Se₂. The initial angle $\theta = 0^\circ$ corresponds to the crystallographic a -axis.

13

14 As illustrated in Fig. 4, monolayer TaNi₂Se₂ exhibits pronounced in-plane mechanical anisotropy. The
15 orientation-dependent Young's modulus $E(\theta)$, shear modulus $G(\theta)$ and Poisson's ratio $\nu(\theta)$ varies
16 nonmonotonically as the direction rotates from $\theta = 0^\circ$ to 90° . Specially, the Young's modulus increases
17 from 98.8 N/m at 0° to a maximum of 124.2 N/m at 45° , and then decreases to 76.8 N/m at 90° . In
18 contrast, the shear modulus decreases from 48.6 N/m at 0° to 29.4 N/m at 45° , before recovering to 48.6
19 N/m at 90° . Meanwhile, the Poisson's ratio decreases from 0.54 to 0.25 between 0° and 45° , and then
20 increases to 0.42 at 90° . The intrinsic Young's modulus of monolayer TaNi₂Se₂ is lower than those of
21 conventional TMDs^[41] but higher than that of anisotropic 2D materials such as black phosphorus (~44
22 N/m).^[42] The combination of relatively high shear rigidity and axial tensile compliance originates from

1 quasi-1D Ta-Ni chain framework, highlighting its potential for application in flexible and strain-
2 engineered nanodevices.

3

4 **Conclusions**

5 We have successfully synthesized quasi-1D monolayer TaNi₂Se₂ via molecular beam epitaxy. Low-
6 temperature STM imaging reveals its characteristic quasi-1D chain-like lattice, while STS measurements
7 confirm the intrinsic metallic nature of the monolayer. Notably, spatially resolved spectroscopy uncovers
8 a pronounced quasi-1D modulation of the electronic states following the chain structure, demonstrating
9 strong electronic anisotropy. First-principles calculations further verify the structural stability of
10 monolayer TaNi₂Se₂ and reveal pronounced in-plane mechanical anisotropy, as well as possible
11 topological edge states induced by SOC. These results establish monolayer TaNi₂Se₂ as a promising
12 quasi-1D vdW material with coupled electronic and mechanical anisotropy, providing a potential
13 platform for future applications in direction-dependent nanomechanical devices^[43] or strain-engineered
14 systems.^[44,45]

15

Accepted Manuscript

1

2 **Experimental methods**

3 *Sample preparation.* Monolayer TaNi₂Se₂ is epitaxially grown on HOPG substrates in an ultra-high-
4 vacuum (UHV) MBE system (base pressure $\sim 5 \times 10^{-10}$ mbar). High-quality HOPG substrate with
5 atomically flat surfaces is obtained by mechanical exfoliation followed by degassing at ~ 870 K for
6 several hours. The monolayer TaNi₂Se₂ is grown by co-evaporating Ta (99.9%, Goodfellow Cambridge
7 Ltd.), Ni (99.95%, Goodfellow Cambridge Ltd.), and Se (99.99%, Sigma-Aldrich) atoms with the
8 substrate maintained at 893 K. The substrate temperature and the Ta/Ni flux ratio must be controlled
9 within an optimized growth window to suppress the formation of other competing quasi-one-
10 dimensional Ta–Ni–Se compounds and thereby obtain a pure TaNi₂Se₂ phase. During growth, the Se flux
11 is kept approximately one order of magnitude higher than the Ta and Ni fluxes to ensure a Se-rich
12 atmosphere. After growth, the sample is kept at 523 K for 30 minutes to remove additional Se.

13

14 *STM/STS characterizations.* After the sample growth, it is then transferred to an STM system via a home-
15 made UHV suitcase. The STM experiments are carried out at 5.7 K in an ultrahigh vacuum (1×10^{-11}
16 mbar) LT-STM systems in the constant current mode with a tungsten tip, which is calibrated on a clean
17 Au(111) surface. STS are acquired by a standard lock-in amplifier at a frequency of 973.1 Hz, under the
18 modulation voltage $V_{\text{mod}} = 20$ mV.

19

20 *DFT calculations.* The calculations of monolayer TaNi₂Se₂ are carried out by using Vienna *ab initio*
21 simulation package (VASP) with the projector augmented wave (PAW) method.^[46] A generalized
22 gradient approximation (GGA) in the form of Perdew-Burke-Ernzerhof (PBE) is adopted for the
23 exchange-correlation functional.^[47] A 20 Å vacuum layer is used, and all atoms are fully relaxed until
24 the residual forces on each atom are smaller than 0.01 eV/Å. The k-points sampling is $12 \times 24 \times 1$ with
25 the Gamma scheme. Wave functions were expanded on a plane-wave basis set up to 500 eV energy cutoff.
26 The fully relaxed lattice constant of monolayer TaNi₂Se₂ is 6.472 Å, 3.452 Å in *a* and *b* direction,
27 respectively. The Wannier functions are constructed using the WANNIER90 code.^[48] The edge-state
28 calculations based on Wannier functions were done using the WannierTools package.^[49] Phonon
29 dispersion is calculated based on supercells larger than 19 Å in the density-functional perturbation theory

1 method implemented in the PHONOPY package.^[50]

2

3

4 **Data availability**

5 Data measured or analyzed during this study are available from the corresponding author on reasonable
6 request.

7

8 **Acknowledgements**

9 This work is supported by grants from the National Key Research and Development Projects of China
10 (2022YFA1204100), the National Natural Science Foundation of China (62488201, 92580202,
11 52572188, 52572063 and 52350322), the CAS Project for Young Scientists in Basic Research (YSBR-
12 053 and YSBR-003), the Fundamental Research Funds for the Central Universities (FRF-TP-24-055A
13 and FRF-IDRY-24-007), and the State Key Lab for Advanced Metals and Materials (41601124 and
14 41601126).

15

16 **Author Contributions:** H.-J.G., H.G., and H.C. designed the experiments. J.W., H.G., and S.X.
17 fabricated the samples. Q.Y., H.C., and P.F. performed STM experiments. Y.X.G. did the DFT
18 calculations. All of the authors participated in analyzing the data, plotting figures, and writing the
19 manuscript.

20

21 **Competing Interests:** The authors declare that they have no competing interests.

References

- [1] Novoselov K S, Geim A K, Morozov S V, Jiang D, Katsnelson M I, Grigorieva I V, Dubonos S V and Firsov A A 2005 *Nature* **438** 197–200
- [2] Zhang Y, Tan Y-W, Stormer H L and Kim P 2005 *Nature* **438** 201–4
- [3] Pan Y, Zhang H, Shi D, Sun J, Du S, Liu F and Gao H-J 2009 *Adv. Mater.* **21** 2777–80
- [4] Guo H, Zhang R, Li H, Wang X, Lu H, Qian K, Li G, Huang L, Lin X, Zhang Y, Ding H, Du S X, Pantelides S T, Gao H-J 2020 *Nano Lett.* **20** 2674
- [5] Ye J T, Zhang Y J, Akashi R, Bahramy M S, Arita R and Iwasa Y 2012 *Science* **338** 1193–6
- [6] Geim A K and Grigorieva I V 2013 *Nature* **499** 419–25
- [7] Guo H, Huang Z, Gao Y, Chen H, Zhang H, Fang Q, Ye Y, Han X, Cao Z, Wang J, Zhou R, Li Z, Shen C, Yang H, Chen H, Yao W, Wang Z and Gao H-J 2025 *Nat. Commun.* **16** 11327
- [8] Liu Z-L, Wu X, Shao Y, Qi J, Cao Y, Huang L, Liu C, Wang J-O, Zheng Q, Zhu Z-L, Ibrahim K, Wang Y-L and Gao H-J 2018 *Sci. Bull.* **63** 419–25
- [9] Kim J, Baik S S, Ryu S H, Sohn Y, Park S, Park B-G, Denlinger J, Yi Y, Choi H J and Kim K S 2015 *Science* **349** 723–6
- [10] Wang G, Bao L, Pei T, Ma R, Zhang Y-Y, Sun L, Zhang G, Yang H, Li J, Gu C, Du S, Pantelides S T, Schrimpf R D and Gao H-J 2016 *Nano Lett.* **16** 6870–8
- [11] Tongay S, Sahin H, Ko C, Luce A, Fan W, Liu K, Zhou J, Huang Y-S, Ho C-H, Yan J, Ogletree D F, Aloni S, Ji J, Li S, Li J, Peeters F M and Wu J 2014 *Nat. Commun.* **5** 3252
- [12] Chenet D A, Aslan B, Huang P Y, Fan C, van der Zande A M, Heinz T F and Hone J C 2015 *Nano Lett.* **15** 5667–72
- [13] Ali M N, Xiong J, Flynn S, Tao J, Gibson Q D, Schoop L M, Liang T, Haldolaarachchige N, Hirschberger M, Ong N P and Cava R J 2014 *Nature* **514** 205–8
- [14] Zhu Y, Wang Z, Ren Y, Yuan P, Chen J, Ou Y, Meng L and Zhang Y 2025 *Chin. Phys. B* **34** 017302
- [15] Lin Y-C, Komsa H-P, Yeh C-H, Björkman T, Liang Z-Y, Ho C-H, Huang Y-S, Chiu P-W, Krasheninnikov A V and Suenaga K 2015 *ACS Nano* **9** 11249–57
- [16] Zhou K, Deng J, Chen L, Xia W, Guo Y, Yang Y, Guo J-G and Guo L 2021 *Chin. Phys. B* **30** 087202
- [17] Wang X, Jones A M, Seyler K L, Tran V, Jia Y, Zhao H, Wang H, Yang L, Xu X and Xia F 2015 *Nat. Nanotechnol.* **10** 517–21

- 1 [18] Aslan B, Chenet D A, van der Zande A M, Hone J C and Heinz T F 2016 *ACS Photonics* **3** 96–
2 101
- 3 [19] Wu W, Wang L, Li Y, Zhang F, Lin L, Niu S, Chenet D, Zhang X, Hao Y, Heinz T F, Hone J and
4 Wang Z L 2014 *Nature* **514** 470–4
- 5 [20] Zhu H, Wang Y, Xiao J, Liu M, Xiong S, Wong Z J, Ye Z, Ye Y, Yin X and Zhang X 2015 *Nat.*
6 *Nanotechnol.* **10** 151–5
- 7 [21] Hellmann S, Rohwer T, Kalläne M, Hanff K, Sohrt C, Stange A, Carr A, Murnane M M, Kapteyn
8 H C, Kipp L, Bauer M and Rossnagel K 2012 *Nat. Commun.* **3** 1069
- 9 [22] Huber T, Mariager S O, Ferrer A, Schäfer H, Johnson J A, Grübel S, Lübcke A, Huber L,
10 Kubacka T, Dornes C, Laulhe C, Ravy S, Ingold G, Beaud P, Demsar J and Johnson S L 2014
11 *Phys. Rev. Lett.* **113** 026401
- 12 [23] Brun C, Wang Z-Z, Monceau P and Brazovskii S 2010 *Phys. Rev. Lett.* **104** 256403
- 13 [24] van Midden M A, van Midden H J P, Prodan A, Bennett J C and Zupanič E 2020 *Phys. Rev. B*
14 **102** 075442
- 15 [25] Zhang H, Chen H, Huang Z, Wang Z-A, Lv S, Xian G, Guo H, Yang H and Gao H-J 2025 *Nano*
16 *Lett.* **25** 16650
- 17 [26] Liu S, Nie S-M, Qi Y-P, Guo Y-F, Yuan H-T, Yang L-X, Chen Y-L, Wang M-X and Liu Z-K 2021
18 *Chin. Phys. Lett.* **38** 077302
- 19 [27] Tan H, Feng Y, Ma X, Wang C, Li R, Wu J, Huang L, Lu Y and Xiang B 2024 *Phys. Rev. Mater.*
20 **8** 104412
- 21 [28] Neuhausen J, Evstafiev V K, Block T, Finckh E W, Tremel W, Augustin L, Fuchs H, Voß D,
22 Krüger P, Mazur A and Pollmann J 1998 *Chem. Mater.* **10** 3870–8
- 23 [29] Jiao W-H, Liu Y, Tao P, Lu J, Liang X, Yang W, Zhang Z, Xu S, Luo Y, Zhu Z-W, Qian D, Xu
24 X, Ren Z, Cao G-H and Xiao S 2025 *Phys. Rev. B* **111** 045109
- 25 [30] Singha R, Yuan F, Cheng G, Salters T H, Oey Y M, Villalpando G V, Jovanovic M, Yao N and
26 Schoop L M 2022 *Adv. Funct. Mater.* **32** 2108920
- 27 [31] Wang L, Tian J, Kang C, Gu H, Pang R, Shen M, She L, Song Y, Liu X and Zhang W 2022
28 *Inorg. Chem.* **61** 18899–906
- 29 [32] Pate S, Chen B, Shen B, Li K, Zhou X, Chung D Y, Divan R, Kanatzidis M G, Welp U, Kwok
30 W-K and Xiao Z-L 2024 *Phys. Rev. B* **109** 035129
- 31 [33] Chhowalla M, Shin H S, Eda G, Li L-J, Loh K P and Zhang H 2013 *Nat. Chem.* **5** 263–75

- 1 [34] Yin Z P, Haule K and Kotliar G 2011 *Nat. Mater.* **10** 932–5
- 2 [35] Imada M, Fujimori A and Tokura Y 1998 *Rev. Mod. Phys.* **70** 1039–263
- 3 [36] Huang J 2000 *Sc. China Ser. B-Chem.* **43** 337–47
- 4 [37] Koma A 1992 *Thin Solid Films* **216** 72–76
- 5 [38] Yu Y, Wang G, Qin S, Wu N, Wang Z Y, He K and Zhang X-A 2017 *Carbon* **115** 526–531
- 6 [39] Huang X, Guan J, Lin Z, Liu B, Xing S, Wang W and Guo J 2017 *Nano Lett.* **17** 4619–4623
- 7 [40] Yu Y, Wang G, Tan Y, Wu N, Zhang X-A and Qin S 2018 *Nano Lett.* **18** 675–681
- 8 [41] Zeng F, Zhang W-B and Tang B-Y 2015 *Chin. Phys. B* **24** 097103.
- 9 [42] Wei Q and Peng X 2014 *Appl. Phys. Lett.* **104** 251915
- 10 [43] Wang Z, Jia H, Zheng X-Q, Yang R, Ye G J, Chen X H and Feng P X-L 2016 *Nano Lett.* **16**
- 11 5394–400
- 12 [44] Qin M-S, Zhu P-F, Ye X-G, Xu W-Z, Song Z-H, Liang J, Liu K and Liao Z-M 2021 *Chin. Phys.*
- 13 *Lett.* **38** 017301
- 14 [45] Ryu Y K, Carrascoso F, López-Nebreda R, Agraït N, Frisenda R and Castellanos-Gomez A 2020
- 15 *Nano Lett.* **20** 5339–45
- 16 [46] Kresse G and Furthmüller J 1996 *Phys. Rev. B* **54** 11169–86
- 17 [47] Perdew J P, Burke K and Ernzerhof M 1996 *Phys. Rev. Lett.* **77** 3865–8
- 18 [48] Mostofi A A, Yates J R, Pizzi G, Lee Y-S, Souza I, Vanderbilt D and Marzari N 2014 *Comput.*
- 19 *Phys. Commun.* **185** 2309–10
- 20 [49] Wu Q, Zhang S, Song H-F, Troyer M and Soluyanov A A 2018 *Comput. Phys. Commun.* **224**
- 21 405–16
- 22 [50] Togo A and Tanaka I 2015 *Scr. Mater.* **108** 1–5
- 23
- 24
- 25